

# Decellularization of Sheep Heart Tissue: A Biocompatible Platform for Tissue Regeneration

Zahra Chavoshi<sup>1</sup>, Asadollah Asadi<sup>1</sup>, Arash Abdolmaleki<sup>\*2</sup>, Saber Zahri<sup>1</sup>, Maryam Jahanvar<sup>1</sup>, Hussein A. Ghanimi<sup>3</sup>

1- Department of Biology, Faculty of Science, University of Mohaghegh Ardabili, Ardabil, Iran.

2- Department of Biophysics, Faculty of Advanced Technologies, University of Mohaghegh Ardabili, Namin, Iran.

3- College of Nursing, University of Al-Ameed, Karbala, Iraq

## Abstract

Tissue engineering (TE) is an evolving discipline aimed at the repair, replacement, or regeneration of injured tissues and organs through the integration of biomaterials, living cells, and bioactive substances. Among the various strategies, the use of acellular scaffolds derived from extracellular matrix (ECM) has shown great promise. These scaffolds, which are devoid of cellular components, retain the structural and biochemical cues necessary for supporting cell adhesion, proliferation, and differentiation. Their inherent biocompatibility and bioactivity make them highly suitable for tissue regeneration applications. In this study, we aimed to develop and evaluate a biocompatible scaffold from sheep heart tissue using a chemical decellularization process. The efficiency of decellularization and preservation of the ECM were assessed through histological staining, DNA quantification, biochemical assays, and scanning electron microscopy (SEM). Results confirmed the effective removal of cellular material while maintaining the ECM architecture. To investigate the scaffold's biocompatibility, adipose-derived mesenchymal stem cells (Ad-MSCs) were seeded onto the decellularized matrix. Cell viability and adhesion were evaluated using MTT assays and SEM imaging. The scaffold supported a high rate of cell viability (88%) and demonstrated favorable cell attachment. These findings highlight the potential of decellularized sheep heart tissue as a reliable, bioactive, and structurally supportive platform for stem cell integration and tissue regeneration. Given its mechanical strength, preserved ECM composition, and excellent

---

\* Corresponding Authors

29 cytocompatibility, this scaffold may serve as a promising candidate for applications in regenerative  
30 medicine and TE, particularly in cardiac and soft tissue repair.

31 **Keywords:** Tissue Engineering, Adipose-Derived Stem Cells (ADSCs), Heart Tissue, Decellularization,  
32 Cardiovascular Regeneration

33

## 34 **1. Introduction**

35 Cardiovascular diseases remain a leading health concern, significantly impacting both life expectancy and  
36 quality of life despite advances in medical treatments and surgical interventions. Recognized as an  
37 emerging epidemic since the mid-1990s, heart failure rates have escalated due to an aging and growing  
38 global population (1,2). Current therapeutic approaches include organ transplantation, surgical  
39 reconstruction, mechanical devices, and metabolic product injections. However, these methods face  
40 challenges, such as immune rejection, the necessity for lifelong immunosuppressive therapy, and  
41 complications arising from device malfunctions or infections (3,4).

42 In recent times, tissue engineering has gained attention as a potential solution for treating cardiovascular  
43 diseases. Decellularized extracellular matrix (d-ECM) is central to regenerative medicine and cardiac TE,  
44 to repair, replace, and regenerate damaged or defective heart tissue. Developing a three-dimensional  
45 scaffold with properties that can modulate cellular activity and behavior for effective regeneration  
46 requires carefully balancing three primary components: cells, scaffolds, and biosignals (5–7). The  
47 extracellular matrix (ECM), produced by cells, forms a complex three-dimensional network of  
48 macromolecules, including structural proteins like collagen, polysaccharides, enzymes, and growth  
49 factors. This network not only defines the tissue's mechanical, chemical, and physical properties but also  
50 influences cellular function (8–11).

51 The cardiac extracellular matrix (ECM) consists of polysaccharides and glycosylated proteins, including  
52 fibrous components such as laminin, fibronectin, and tenascin, each fulfilling a distinct function. This  
53 natural ECM, produced by the heart's cells, facilitates communication between cells and their  
54 surroundings, influencing vital processes such as cell movement, development, and death. However,  
55 replicating this complex ECM in a laboratory setting is challenging. To address this, researchers use  
56 tissue decellularization, a technique that removes cells but preserves the ECM's structure, reducing the  
57 risk of immune rejection (4,6,12).

58 Decellularization protocols often use enzymatic, chemical, and physical techniques. Standard physical  
59 methods include freeze-thaw cycles and mechanical forces to break down cell membranes; however, these

60 can damage the ECM due to ice crystal formation or mechanical stress. Enzymatic methods, which use  
61 nucleases and proteases to degrade cellular components such as RNA, DNA, and proteins, may also  
62 disrupt the ECM. Chemical methods widely involve the use of non-ionic or ionic detergents for cell  
63 removal. For example, Triton X-100 (non-ionic) preserves protein-protein interactions, while SDS (ionic)  
64 effectively solubilizes cell membranes, though prolonged exposure can alter ECM structure. Tailoring  
65 decellularization protocols to each tissue type is essential to maintain ECM integrity across different  
66 organs (13–15).

67 In this study, we evaluated chemical methods for preparing decellularized sheep heart scaffolds, focusing  
68 on the importance of optimized washing steps. By comparing the molecular and cellular properties of the  
69 prepared scaffolds to untreated controls, we aimed to verify the effectiveness of the decellularization  
70 process in preserving the extracellular matrix (ECM) structure while ensuring complete cell removal.  
71 We conducted detailed analyses on the samples to confirm ECM integrity and the absence of cellular  
72 remnants. Additionally, we performed MTT assays to assess the *in vitro* biocompatibility of the  
73 decellularized scaffolds, examining cell viability and survival when cultured on the ECM. This  
74 comprehensive approach ensures that the decellularized ECM provides a safe and supportive environment  
75 for future cell seeding and tissue engineering applications.

## 76 **2. Methods and material**

### 77 2.1. Ethics approval

78 All experimental procedures were performed in accordance with the European Union Council Directive  
79 of November 24, 1986, and were approved by the Ethics Committee of the University of Mohagheh  
80 Ardabili (IR.UMA.REC.1400.084).

### 81 2.2. Scaffold Preparation

82 For this study, sheep heart tissue (n = 3) was harvested immediately after slaughter from a local  
83 slaughterhouse, following ethical protocols. The heart tissue, rich in vascular structures, was selected for  
84 its suitability for decellularization. A chemical decellularization approach was utilized, involving 0.5%  
85 sodium deoxycholate (Sigma-Aldrich), 0.5% sodium dodecyl sulfate (SDS, Sigma-Aldrich), and  
86 phosphate-buffered saline (PBS, Gibco). The heart tissue was sectioned into 3 mm thick slices, measuring  
87 approximately 2x2 cm. These sections were washed with distilled water, followed by three 10-minute  
88 washes in PBS to remove residual blood and debris. The tissue samples were then immersed in a solution  
89 containing 0.5% SDS and 0.5% sodium deoxycholate for 24 hours to facilitate cellular removal.  
90 Following decellularization, the tissues underwent six successive washes with PBS, spaced 12 hours

91 apart, to eliminate any remaining detergents and cellular debris. After decellularization, the samples and  
92 control tissues were stored in PBS and examined morphologically to assess ECM integrity and confirm  
93 effective cell removal.

### 94 2.3. The Histological Analysis

95 To assess the histological characteristics of the decellularized scaffolds, including cell removal and  
96 extracellular matrix preservation, both the control (n = 5) and scaffold (n = 5) samples were fixed in  
97 10% formalin (Sigma-Aldrich). Each sample was sectioned into 5-micrometer slices and embedded in  
98 paraffin. Hematoxylin and eosin staining (H&E staining kit, Sigma-Aldrich) was performed on the  
99 sections to evaluate the efficiency of cell elimination and the structural integrity of the ECM following  
100 decellularization. The effectiveness of DNA removal was assessed using 4',6-diamidino-2-phenylindole  
101 staining (DAPI staining kit, Sigma-Aldrich). DAPI binds to adenine-thymine (A-T) rich regions of  
102 double-stranded DNA, allowing for clear visualization of any remaining nuclei in the decellularized  
103 samples. To verify the preservation of collagen filaments, the most abundant protein filaments in the  
104 cardiac ECM, Masson's trichrome staining (Masson's trichrome staining kit, Sigma-Aldrich) was  
105 employed. This staining method highlights the collagen structures within the scaffold, providing a  
106 detailed assessment of ECM integrity post-decellularization.

### 107 2.4. Ultrastructural Evaluation

108 The ultrastructural preservation of the decellularized scaffolds was evaluated by SEM (SEM, SU4800,  
109 Japan). Samples from both the control group (n = 4) and the decellularized scaffolds (n = 4) were first  
110 fixed in 2.5% glutaraldehyde (Sigma-Aldrich) for 24 hours. Following fixation, the samples were  
111 dehydrated through graded ethanol (Sigma-Aldrich) series (30%, 50%, 70%), with a final immersion in  
112 100% ethanol. Once fully dehydrated, the samples were air-dried to ensure complete moisture removal.  
113 The dried samples were coated with a thin layer of gold. The ultrastructural features of the scaffolds were  
114 then captured using SEM, allowing for a detailed evaluation of the scaffold's surface morphology and  
115 structural preservation following the decellularization process.

### 116 2.5. DNA Quantification

117 To quantify the DNA content, 20 mg of both control (n = 3) and decellularized (n = 3) tissue samples  
118 were precisely weighed. The tissue was then digested by adding 5  $\mu$ L of proteinase K (Qiagen) per  
119 milliliter of digestion buffer. The scaffold and control samples were homogenized and incubated in a bain-  
120 marie at 55°C overnight.

121 After incubation, the supernatant was carefully transferred to fresh tubes. Sodium acetate (Merck) was  
122 added to each sample, thoroughly mixed by inversion, and incubated at  $-20^{\circ}\text{C}$  for 15 min to facilitate  
123 protein and cell debris precipitation. The samples were centrifuged at maximum speed for 2 minutes using  
124 an Eppendorf centrifuge, after which the supernatant was carefully collected into fresh tubes.

125 Two volumes of 98% ethanol were added to the supernatant to precipitate nucleic acids, followed by  
126 gentle inversion to mix. The samples were incubated at  $-20^{\circ}\text{C}$  for 15 min, then centrifuged at 6000 rpm  
127 for 20 minutes at  $4^{\circ}\text{C}$ . Then were washed with 98% ethanol and twice with 70% ethanol for air-dry.

128 The dried pellets were resuspended in injection-grade water, and the DNA concentration in the  
129 decellularized and control samples was measured using a Nanodrop spectrophotometer (Termo scientific  
130 USA-Termo One C) at a wavelength of 260 nm, with results expressed in ng/mg (16).

#### 131 2.6. Glycosaminoglycan (GAG) Quantification

132 A Glycosaminoglycan Quantification Kit (Kazist, Iran) was used to evaluate the preservation of  
133 glycosaminoglycans (GAGs) in the decellularized scaffold samples. Scaffold samples ( $n = 3$ ) and control  
134 samples ( $n = 3$ ), each weighing 15 mg, were prepared and placed in 1.5 mL microtubes. Following the  
135 kit's instructions, 400  $\mu\text{L}$  of enzyme solution was added to each microtube, and the samples were  
136 incubated at  $65^{\circ}\text{C}$  in a bain-marie for 16 hours.

137 After incubation, the microtubes were individually weighed for alignment in the centrifuge and  
138 subsequently centrifuged at 6000 rpm for 15 minutes at  $4^{\circ}\text{C}$ . The supernatant was then carefully  
139 transferred to new microtubes, and 50  $\mu\text{L}$  of a protein precipitant was added, followed by an additional  
140 centrifugation step under the same conditions. After centrifugation, 30  $\mu\text{L}$  of each sample was pipetted  
141 into the wells of a 96-well plate, followed by the addition of 200  $\mu\text{L}$  of GAG reagent to each well. Optical  
142 absorbance was measured at 560 nm using an ELISA reader (BioTek EIA reader), according to the  
143 manufacturer's protocol. A standard curve was created using Excel software, and the GAG concentration  
144 in the samples was calculated in  $\text{mg}/\mu\text{g}$ .

#### 145 2.7. Total protein quantification

146 For total protein quantification, Coomassie Brilliant Blue reagent (Sigma-Aldrich) was prepared by  
147 dissolving 10 mg of the dye in 5 mL of 95% ethanol, followed by the addition of 10 mL of 85%  
148 orthophosphoric acid (Sigma-Aldrich). The mixture was then diluted to a final volume of 100 mL with  
149 distilled water and stored refrigerated. A bovine serum albumin (BSA) standard solution (Sigma-Aldrich)  
150 was prepared by dissolving 1 mg of BSA in distilled water to a total volume of 10 mL, yielding a  
151 concentration of 10 mg/mL. For experimental analysis, 0.2 g of decellularized scaffold ( $n = 6$ ) and control

152 (n = 6) tissue were weighed and washed with PBS. The samples were centrifuged at 4000 rpm, and the  
153 buffer was replaced after each spin. In the next step, 150  $\mu$ L of PBS containing 0.1 M DTT (Sigma-  
154 Aldrich) was added to each sample, and they were subjected to three freeze-thaw cycles using liquid  
155 nitrogen to disrupt the tissue. After each thaw, samples were vortexed to ensure complete tissue  
156 homogenization. The supernatant was collected for protein analysis following centrifugation at 1200 rpm  
157 and 4°C.

158 Protein quantification was performed by mixing 20  $\mu$ L of each supernatant with 180  $\mu$ L of Bradford  
159 reagent in a 96-well plate. Absorbance was measured at 595 nm using an ELISA reader, and protein  
160 concentrations were determined by comparing the readings to a BSA standard curve prepared in Excel.

## 161 2.8. Cell culture

162 Adipose-derived mesenchymal stem cells (Ad-MSCs), obtained from the Iranian Biological Resource  
163 Center, were incubated (Memmert IPP750plus) at 37 °C with 95% humidity and 5% CO<sub>2</sub>. After 24 hours,  
164 cells were passaged using 0.25% Trypsin-EDTA (Gibco) and divided into three flasks. The flasks were  
165 monitored daily, with the medium replaced every 48 hours to maintain optimal conditions and remove  
166 dead cells or debris. The cells were grown in a low-glucose DMEM medium (Gibco), supplemented with  
167 20% FBS (Gibco) and 1% penicillin-streptomycin solution (Sigma) to ensure optimal proliferation and  
168 sterility. Adipose-derived mesenchymal stem cells (Ad-MSCs) at the second passage were utilized for  
169 biocompatibility testing. Cell viability was assessed via the MTT assay, and cell adhesion was examined  
170 using scanning electron microscopy (SEM), providing valuable information on scaffold compatibility  
171 (17).

## 172 2.9. Assessment of Cell Viability

173 The cell viability assay is based on reducing MTT tetrazolium salt (Sigma, MO, US) to purple formazan  
174 crystals by the oxidoreductase enzyme present in the mitochondria of viable cells. This color change  
175 indicates cellular viability and the functional presence of the oxidoreductase enzyme.

176 For the cell viability assay, circular segments of the decellularized heart scaffolds, each measuring 0.5 cm  
177 in diameter, were prepared. These scaffolds were sterilized using a 0.5% penicillin-streptomycin solution  
178 in phosphate-buffered saline (PBS), followed by ultraviolet (UV) irradiation for 20 minutes. To verify  
179 sterility, scaffolds were incubated in DMEM medium enriched with 10% FBS for 24 hours at 37°C , 5%  
180 CO<sub>2</sub>. After confirming sterility, the scaffolds were transferred into a 96-well culture plate and seeded with  
181 Ad-MSCs at a density of 10<sup>4</sup> cells per scaffold. For the control group, an equal number of Ad-MSCs were  
182 cultured directly in wells without scaffolds. The plates were then incubated at 37°C, 5% CO<sub>2</sub> for 24 hours.

183 Following incubation, 20  $\mu$ L of MTT reagent was added to each well, and the plates were shielded with  
184 aluminum foil and incubated for another 4 hours. After this, the supernatant containing the MTT reagent  
185 was removed, and 200  $\mu$ L of dimethyl sulfoxide (DMSO; Merck) was introduced to dissolve the resulting  
186 formazan crystals. The plates were then left for 10 minutes before absorbance was measured at 630 nm  
187 using a microplate reader to assess cell viability. The percentage of viable cells was calculated relative to  
188 the control (monolayer culture) using the formula:

$$189 \text{ Cell viability (\%)} = (\text{Mean OD of sample} / \text{Mean OD of control}) \times 100$$

190

### 191 2.10. Assessment of Cell Adhesion

192 After 24 hours of stem cell culture on the scaffolds, tissue fixation was initiated using a 2.5%  
193 glutaraldehyde solution in a saline buffer adjusted to a pH of 7.4. The culture medium was carefully  
194 removed, and the glutaraldehyde solution was applied to the tissue samples, which were then incubated  
195 for 48 hours to ensure effective preservation. To achieve thorough fixation of cellular and scaffold  
196 structures, this step was repeated, followed by an additional 24-hour immersion in the fixative.

197 Subsequent to the fixation process, the glutaraldehyde solution was drained, and the samples were rinsed  
198 three times with the same solution to remove excess fixative. The tissues then underwent a graded ethanol  
199 dehydration sequence, with sequential immersions in 30%, 50%, and 70% ethanol for 15 minutes each.  
200 The complete dehydration was achieved through a final immersion in 100% ethanol. The samples were  
201 then allowed to air-dry completely.

202 Once dried, a thin layer of gold was applied to the samples to enhance surface conductivity, a necessary  
203 step for imaging. The prepared samples were analyzed using scanning electron microscopy (SEM) at an  
204 accelerating voltage of 15 kV and a magnification of 500x to examine detailed surface morphology and  
205 the interactions between the scaffolds and the seeded cells.

### 206 2.11. Data Analysis

207 Results are expressed as mean  $\pm$  SEM. Statistical differences among multiple groups were assessed using  
208 one-way analysis of variance (ANOVA), while comparisons between two groups were made using the t-  
209 test. A p-value below 0.05 ( $p < 0.05$ ) was considered indicative of statistical significance. All statistical  
210 tests and graphical representations were conducted using GraphPad Prism version 8.2.1.

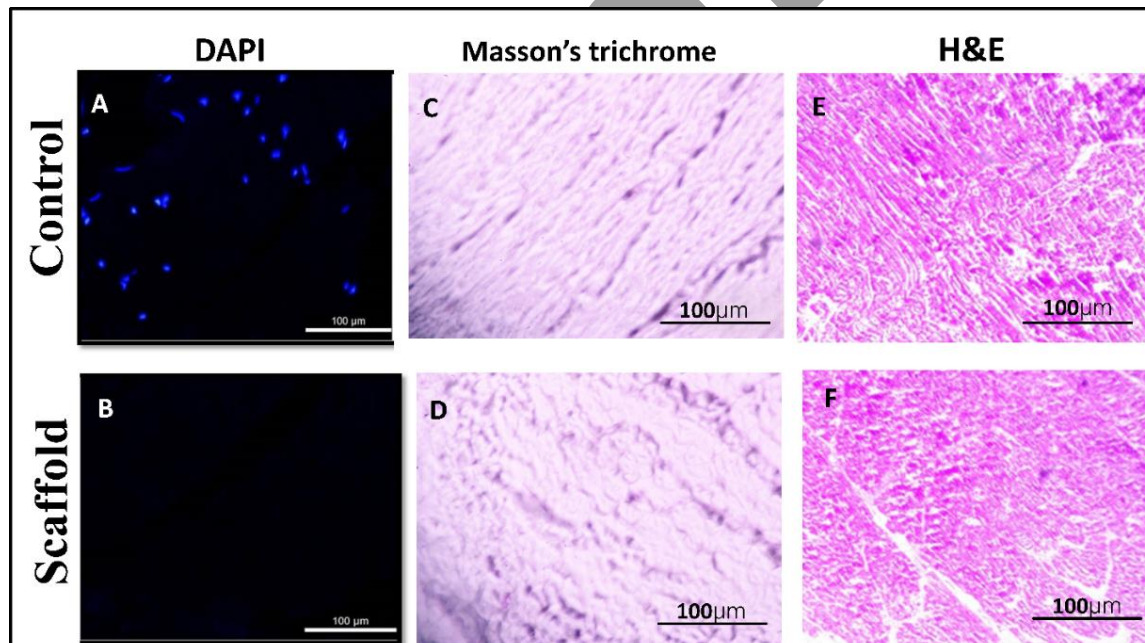
## 211 3. Results

### 212 3.1. Scaffold Characterization

213 DAPI (4',6-diamidino-2-phenylindole) staining was used to detect residual nuclear material. DAPI, a  
214 fluorescent dye that binds specifically to adenine-thymine-rich regions of DNA, is often used in  
215 fluorescence microscopy. Control samples exhibited bright blue fluorescence, indicating nuclear presence,  
216 whereas the absence of fluorescence in treated samples confirmed the effective elimination of nuclear  
217 material during decellularization (Fig. 1 A, B).

218 To further examine the extracellular matrix (ECM), Masson's trichrome staining was performed to  
219 highlight collagen fibers, a primary structural element of the ECM. Results showed that the collagen  
220 network remained intact, suggesting that the decellularization process preserved ECM architecture  
221 without significant disruption (Fig. 1 C, D).

222 Additionally, Hematoxylin and eosin (H&E) staining confirmed the absence of cellular material within  
223 the scaffolds. H&E is a widely used histological technique, where eosin, an acidic dye, stains the  
224 cytoplasm and other acidophilic components pink, and hematoxylin, a basic dye, stains basophilic  
225 structures such as DNA and RNA blue or purple. In the analyzed samples, cytoplasm appeared pink and  
226 nuclei purple, confirming successful cell removal from the scaffolds (Fig. 1 E, F).



227

228 **Fig. 1. Evaluation of cellular content removal and extracellular matrix preservation in decellularized sheep-**  
229 **heart scaffolds. (A, B) DAPI staining of nuclei, where A shows the control sample with visible nuclear staining**  
230 **(blue fluorescence) and B shows the scaffold after decellularization, indicating the absence of nuclear material. (C,**  
231 **D) Masson's trichrome staining, highlighting collagen fibers. C depicts the control sample, while D shows the**



232 scaffold, confirming the retention of collagen structures with no observable cellular content. **(E, F)** Hematoxylin and  
233 eosin (H&E) staining, demonstrating the general tissue morphology. E illustrates the presence of cells in the control  
234 sample, while F shows the scaffold with the removal of cells, yet preservation of the extracellular matrix. Scale bars:  
235 100  $\mu\text{m}$ .

236

237

238

### 239 3.2. DNA Quantification

240 The DNA quantification data from the control tissue sample indicated a DNA content of  $3.33 \pm 0.58$   
241  $\text{ng}/\mu\text{l}$ , reflecting the presence of substantial cellular and nucleic acid material. In contrast, the scaffold  
242 tissue sample demonstrated a significant reduction in DNA content, measuring only  $0.56 \pm 0.58 \text{ ng}/\mu\text{l}$  ( $P =$   
243  $0.0089$ ). This substantial decrease highlights the efficacy of the decellularization process, which  
244 successfully removed nearly all cellular components and nucleic acid residues (Fig. 2 A).

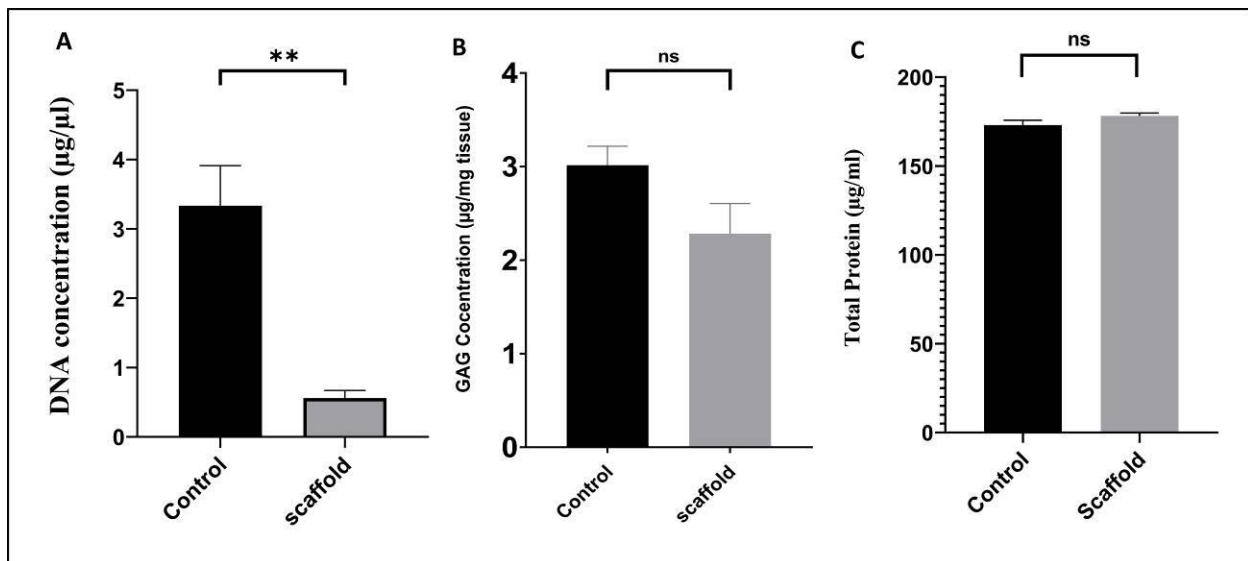
### 245 3.3. GAG and Total Protein Quantification

246 Quantifying glycosaminoglycans (GAGs) and total protein content is crucial for scaffold characterization,  
247 given their roles in cytokine production, activation of signaling molecules, providing extracellular matrix  
248 elasticity and strength, and facilitating nutrient and metabolite diffusion. The control tissue samples,  
249 contained  $3.01 \pm 0.38 \mu\text{g}/\text{mg}$  of GAGs, reflecting the intact extracellular matrix structure. The  
250 decellularized scaffold sample exhibited a slightly lower GAG content of  $2.28 \pm 0.38 \mu\text{g}/\text{mg}$ , with no  
251 significant reduction observed. This minor decrease indicates substantial GAG retention following the  
252 decellularization process (Fig. 2B).

253 Total protein quantification of the control tissue revealed a protein content of  $173.1 \pm 1.696 \mu\text{g}/\text{mg}$ . In  
254 comparison, the scaffold sample indicated a comparable protein content of  $178.2 \pm 1.696 \mu\text{g}/\text{mg}$ ,  
255 indicating no significant difference between the two. These results suggest that the decellularization  
256 method preserved a considerable amount of protein content within the scaffold tissue (Fig. 2C).

257

258



259

260 **Fig. 2. Quantitative analysis of DNA, glycosaminoglycan (GAG), and total protein content in control and**  
 261 **decellularized sheep-heart scaffolds. (A)** DNA concentration was measured in three independent experiments  
 262 (n=3). The results shows a significant reduction in the scaffold group compared to the control, indicating effective  
 263 removal of cellular DNA during the decellularization process (\*\* P < 0.01). **(B)** GAG concentration reveals no  
 264 significant difference (ns) between the control and scaffold groups, suggesting preservation of glycosaminoglycans.  
 265 **(C)** Total protein content analysis indicates no significant difference (ns) between control and scaffold groups,  
 266 confirming the retention of key protein components. Data are presented as mean ± SEM.

267

268

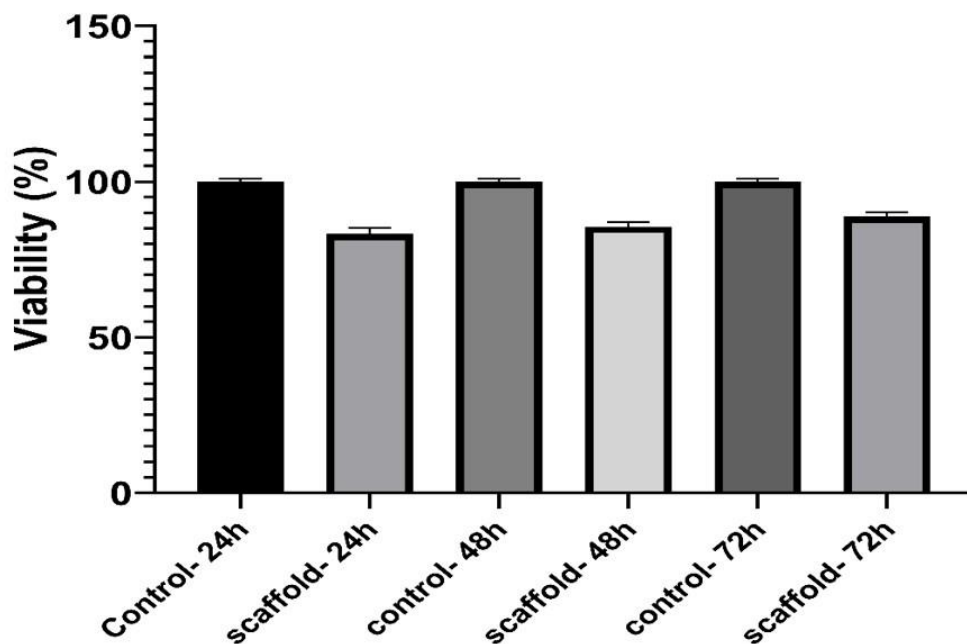
### 269 3.4. Biocompatibility Evaluation

270 Biocompatibility of the decellularized sheep-heart scaffolds was evaluated by performing an MTT assay  
 271 to measure the viability of AD-MSCs seeded onto the scaffolds at 24, 48, and 72 hours after seeding. The  
 272 results demonstrated an increase in cell viability over time, with 83% viability at 24 hours, 85% at 48  
 273 hours, and 88% at 72 hours. These outcomes indicated that the scaffolds provided effective support for  
 274 cell attachment, proliferation, and growth. Moreover, no significant differences in cell viability were  
 275 observed when compared to the control group (monolayer cell culture in media), underscoring the high  
 276 biocompatibility of the decellularized scaffolds. These findings demonstrated the potential of these  
 277 scaffolds as a supportive and conducive matrix for stem cell activity, which is critical for applications in  
 278 tissue engineering (Fig. 3).

279 Further evidence from scanning electron microscopy (SEM) imaging demonstrated strong adhesion of  
 280 adipose-derived mesenchymal stem cells (AD-MSCs) to the surfaces of the decellularized scaffolds (Fig.

281 4). This observation underscores the scaffold's capacity to support effective cell attachment, highlighting  
282 its potential as a highly biocompatible environment conducive to stem cell development, proliferation,  
283 and sustained viability.

284

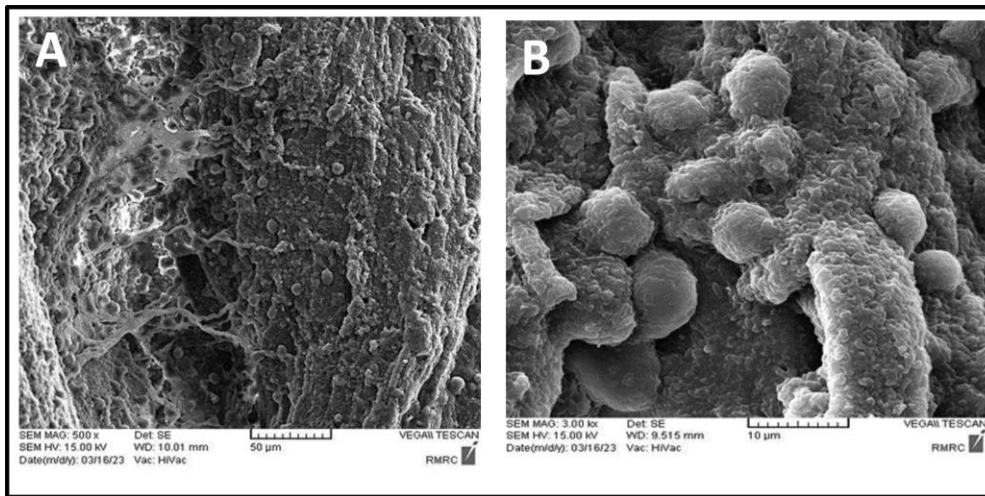


285

286 **Fig. 3. Biocompatibility assessment of decellularized sheep-heart scaffolds using the MTT assay.** The viability  
287 of adipose-derived mesenchymal stem cells (AD-MSCs) seeded on the decellularized heart scaffolds was measured  
288 at 24, 48, and 72 hours post-seeding. The results showed an increase in cell viability over time, with 83% at 24  
289 hours, 85% at 48 hours, and 88% at 72 hours. No significant differences in cell viability were observed when  
290 compared to the control group (monolayer cell culture in media).

291

292



293  
294 **Fig. 4. Scanning electron microscopy (SEM) images showing the adhesion of adipose-derived mesenchymal**  
295 **stem cells (AD-MSCs) on the surface of decellularized sheep-heart scaffolds. (A) SEM image taken 24 hours**  
296 **after cell seeding at 500x magnification, with a scale bar of 50  $\mu$ m, demonstrating initial cell attachment on the**  
297 **scaffold surface. (B) SEM image taken 48 hours after cell seeding at 500x magnification, with a scale bar of 10  $\mu$ m,**  
298 **showing enhanced cell adhesion and spreading. Both images were captured at a voltage of 15 kV.**

299

300

#### 301 **4. Discussion**

302 In cardiac tissue engineering and regenerative medicine, the utilization of decellularized extracellular  
303 matrix (d-ECM) has garnered significant attention as a viable strategy for the repair, replacement, and  
304 regeneration of damaged or dysfunctional cardiac tissue. Central to this approach is the fabrication of a  
305 three-dimensional scaffold designed to modulate cellular behavior and promote functional tissue  
306 restoration. The success of this process hinges upon the synergistic integration of three fundamental  
307 components: the scaffold framework, appropriate cellular populations, and bioactive signaling factors  
308 (18,19). The ECM is a sophisticated and dynamic three-dimensional scaffold, primarily made up of  
309 structural proteins like collagen, alongside various enzymes, signaling molecules, and polysaccharides.  
310 This matrix is synthesized and released by local cells, and it creates a unique microenvironment that  
311 facilitates cell attachment, growth, movement, and specialization. Furthermore, the ECM contributes to  
312 the tissue's unique physical, chemical, and biomechanical features that are crucial for its proper function  
313 (20,21). The cardiac ECM predominantly consists of glycosylated proteins and polysaccharides,  
314 encompassing fibrous proteins such as laminin, tenascin, and fibronectin, each of which plays distinct and  
315 critical roles in maintaining the structural and functional integrity of the tissue microenvironment (22).

316 The native ECM, synthesized by resident cardiac cells, provides a biologically active and naturally  
317 functionalized scaffold that facilitates critical cell–cell and cell–matrix interactions. These interactions are  
318 essential for regulating cellular processes such as migration, differentiation, and apoptosis, ultimately  
319 influencing tissue homeostasis and repair (23). Due to the intricate biochemical and structural  
320 composition of natural ECM, replicating its full complexity through synthetic means remains a significant  
321 challenge. Consequently, a growing body of research has turned toward the use of decellularized tissues  
322 to generate biologically derived ECM scaffolds. These scaffolds aim to preserve the native three-  
323 dimensional architecture and biochemical cues of the ECM while effectively removing immunogenic  
324 cellular components to minimize the risk of immune rejection in regenerative applications (24).

325 However, several challenges remain in optimizing the decellularization and recellularization processes.  
326 Complete removal of cellular antigens is necessary to minimize immune responses, while maintaining  
327 ECM integrity is crucial for mechanical stability and biological functionality. Additionally, the  
328 repopulation of decellularized matrices with appropriate cell types, including endothelial cells,  
329 cardiomyocytes, and supporting stromal cells, remains a complex and tightly regulated process.  
330 Advancements in stem cell technologies, bioreactor systems, and gene editing tools may help overcome  
331 these limitations and enhance the functionality of bioengineered cardiac tissues (25).

332 Effective decellularization protocols commonly integrate enzymatic, chemical, and physical methods to  
333 ensure thorough cellular removal while minimizing damage to the extracellular matrix (ECM). Physical  
334 techniques—such as freeze-thaw cycles and mechanical agitation—are typically employed as supportive  
335 measures to facilitate cell lysis but can compromise ECM integrity due to ice crystal formation and  
336 mechanical stress (26). Enzymatic approaches, utilizing nucleases and proteases, are efficient at  
337 degrading nucleic acids and cellular proteins; however, if not precisely controlled, they may inadvertently  
338 disrupt ECM components (27). Chemical methods remain the most widely applied, particularly those  
339 employing detergents such as Triton X-100 and SDS, due to their effectiveness in solubilizing cell  
340 membranes. Nevertheless, extended exposure to these detergents—especially SDS—can result in protein  
341 denaturation and ECM degradation. To preserve the biochemical and mechanical properties of the matrix,  
342 it is therefore advisable to limit the duration of detergent exposure (28).

343 In this study, we adopted a chemical decellularization strategy using sheep heart tissue, leveraging the  
344 anatomical and physiological similarities between sheep and humans. Compared to smaller animal  
345 models, sheep hearts offer a more clinically relevant platform for translational research, and their  
346 comparable size facilitates the development of scalable tissue engineering protocols (29,30). Moreover,  
347 we propose an optimized decellularization protocol for cardiac tissue based on a synergistic combination  
348 of Triton X-100 and SDS, applied over a shortened incubation period to minimize ECM disruption.

349 The efficacy of the decellularization protocol was validated through both histological and biochemical  
350 assessments. DAPI staining confirmed the complete absence of nuclear material, while hematoxylin and  
351 eosin (H&E) staining demonstrated effective removal of cellular components with preservation of the  
352 extracellular matrix (ECM) architecture. Masson's trichrome staining further revealed intact collagen  
353 fibers, underscoring the structural integrity of the decellularized scaffold. Biochemical analyses  
354 corroborated the histological findings. Quantification of glycosaminoglycans (GAGs) showed a slight,  
355 non-significant reduction in content, indicating that essential biomechanical characteristics were largely  
356 preserved. Total protein analysis similarly revealed no significant differences between native and  
357 decellularized tissues, highlighting the protocol's ability to maintain key structural proteins critical for  
358 supporting recellularization and tissue regeneration. These findings are consistent with previous studies  
359 demonstrating the potential of decellularized scaffolds to support recellularization and functional tissue  
360 regeneration. For instance, in the study by Lu et al. (2013), the decellularized heart matrix provided a  
361 biologically relevant environment that facilitated the engraftment, differentiation, and organization of  
362 human cardiovascular progenitor cells, ultimately promoting the formation of functional cardiac tissue  
363 (31).

364 Biocompatibility is crucial for scaffold evaluation, and our results showed that the decellularized sheep-  
365 heart scaffolds provided a conducive environment for cell viability and growth. The MTT assay revealed  
366 no significant difference in stem cells viability between the scaffold and control samples. Furthermore,  
367 SEM imaging confirmed successful cell attachment, reinforcing the scaffold's potential for supporting  
368 cell adhesion, proliferation, and differentiation. These findings indicate that our decellularized scaffolds  
369 are well-suited for use in cardiac tissue engineering. This results are consistent with previous studies. Ott  
370 et al. (2008) were pioneers in demonstrating the functional recellularization of decellularized cardiac  
371 scaffolds, achieving pump-like activity with reseeded murine heart tissues (32). Weymann and colleagues  
372 expanded this work by developing decellularized porcine heart scaffolds, preserving crucial ECM features  
373 and achieving partial recellularization. Although challenges such as incomplete endothelialization remain,  
374 advancements continue to refine decellularization and recellularization strategies (33).

375 Nevertheless, certain limitations must be acknowledged. While detergents like SDS are highly effective at  
376 removing cellular content, they can disrupt the ECM ultrastructure if not carefully controlled. Optimizing  
377 detergent concentration and exposure time is crucial to minimizing this damage. research should explore  
378 alternative decellularization techniques. Additionally, we did not perform mechanical testing in this study,  
379 but we recommend that future research include such assessments. In conclusion, our study demonstrates  
380 that decellularized sheep-heart scaffolds retain essential ECM components, exhibit high biocompatibility,  
381 and provide a robust platform for cardiac tissue engineering. Continued research into scaffold

382 optimization and effective recellularization strategies will be crucial for advancing these constructs  
383 toward organ repair and regeneration, bringing them closer to clinical application.

#### 384 **Acknowledgements**

385 The authors are grateful for the support provided by the University of Mohaghegh Ardabili.

#### 386 **Authors' contributions**

387 A. Ab collaborated on the conception, design, and planning of the study. A. Ab, A. As conducted the  
388 literature review, while Z. Ch , M. J, S. Z, reviewed the selected studies, assessed their quality, and  
389 gathered the required data. S. Z, A. Ab, A. As, M. J, Z. Ch, H A.G performed the statistical analyses and  
390 drafted the initial manuscript. All authors contributed to the interpretation of the results, provided critical  
391 revisions, and approved the final version of the manuscript for publication.

#### 392 **Conflict of Interest**

393 The authors declare no conflict of interest in this study

#### 394 **Funding statement**

395 This research received no specific grant from any funding agency in the public, commercial, or not-for-  
396 profit sectors.

#### 397 **Data availability**

398 All data generated or analyzed during this study are included in this article. Further enquiries can be  
399 directed to the corresponding author.

#### 400 **Ethics**

401 All experimental procedures were performed in accordance with the European Union Council Directive  
402 of November 24, 1986, and were approved by the Ethics Committee of the University of Mohaghegh  
403 Ardabili (IR.UMA.REC.1400.084).

404

#### 405 **References**

- 406 1. Roger VL. Epidemiology of Heart Failure. *Circ Res* [Internet]. 2021 May 14;128(10):1421–34. Available  
407 from: <https://www.ahajournals.org/doi/10.1161/CIRCRESAHA.121.318172>
- 408 2. Buckley JP. The changing landscape of cardiac rehabilitation; from early mobilisation and reduced mortality  
409 to chronic multi-morbidity management. *Disabil Rehabil* [Internet]. 2021 Nov 20;43(24):3515–22. Available  
410 from: <https://www.tandfonline.com/doi/full/10.1080/09638288.2021.1921062>
- 411 3. Shibasaki I, Otani N, Saito S, Ogawa H, Masawa T, Tsuchiya G, et al. Overview of mechanical circulatory  
412 support for the management of post-myocardial infarction ventricular septal rupture. *J Cardiol* [Internet].

- 413 2023 May;81(5):491–7. Available from: <https://linkinghub.elsevier.com/retrieve/pii/S0914508722003094>
- 414 4. Belviso I, Sacco AM, Cozzolino D, Nurzynska D, Di Meglio F, Castaldo C, et al. Cardiac-derived  
415 extracellular matrix: A decellularization protocol for heart regeneration. Limana F, editor. PLoS One  
416 [Internet]. 2022 Oct 19;17(10):e0276224. Available from: <https://dx.plos.org/10.1371/journal.pone.0276224>
- 417 5. Nair A, Nadine S, Ahadian S, Mano J, Tanideh N, Thankam FG. Translational tissue engineering. In: Tissue  
418 Engineering [Internet]. Elsevier; 2022. p. 557–73. Available from:  
419 <https://linkinghub.elsevier.com/retrieve/pii/B978012824064900023X>
- 420 6. Kafili G, Kabir H, Jalali Kandeloo A, Golafshan E, Ghasemi S, Mashayekhan S, et al. Recent advances in  
421 soluble decellularized extracellular matrix for heart tissue engineering and organ modeling. J Biomater Appl  
422 [Internet]. 2023 Nov 24;38(5):577–604. Available from:  
423 <https://journals.sagepub.com/doi/10.1177/08853282231207216>
- 424 7. kohgard sedighe, Zahri S, latifi saeid, Jahanvar maryam. Downregulation of EPHA2 by Helicobacter  
425 pylori in Gastric Epithelial Cells: Implications for Gastric Cancer Progression. J Cell Mol Res [Internet].  
426 2025; Available from: [https://jcmr.um.ac.ir/article\\_47173.html](https://jcmr.um.ac.ir/article_47173.html)
- 427 8. Whitehead KM, Hendricks HKL, Cakir SN, de Castro Brás LE. ECM roles and biomechanics in cardiac  
428 tissue decellularization. Am J Physiol Circ Physiol [Internet]. 2022 Sep 1;323(3):H585–96. Available from:  
429 <https://journals.physiology.org/doi/10.1152/ajpheart.00372.2022>
- 430 9. Neishabouri A, Soltani Khaboushan A, Daghigh F, Kajbafzadeh AM, Majidi Zolbin M. Decellularization in  
431 Tissue Engineering and Regenerative Medicine: Evaluation, Modification, and Application Methods. Front  
432 Bioeng Biotechnol [Internet]. 2022 Apr 25;10. Available from:  
433 <https://www.frontiersin.org/articles/10.3389/fbioe.2022.805299/full>
- 434 10. Khashjoori B, Ghamsari SM, Dehghan MM, Farzad Mohajei S, Gholami H, Golshahi H. Evaluation of the  
435 Effects of Adipose Derived Mesenchymal Stem Cells Cultured on Decellularized Amniotic Membrane in  
436 Wound Healing of Distal Part of the Limbs in Horse. Iran J Vet Med [Internet]. 2019;13(1):11–25. Available  
437 from: [https://ijvm.ut.ac.ir/article\\_70105.html](https://ijvm.ut.ac.ir/article_70105.html)
- 438 11. Hamza AA, Ismail Ibrahim Z. Role of Tumor Necrosis Factor- $\alpha$  in Experimental Streptococcus pneumoniae  
439 Infection in Lambs. Iran J Vet Med [Internet]. 2025;19(1):11–22. Available from:  
440 [https://ijvm.ut.ac.ir/article\\_100614.html](https://ijvm.ut.ac.ir/article_100614.html)
- 441 12. Hochman-Mendez C, Pereira de Campos DB, Pinto RS, Mendes BJ da S, Rocha GM, Monnerat G, et al.  
442 Tissue-engineered human embryonic stem cell-containing cardiac patches: evaluating recellularization of  
443 decellularized matrix. J Tissue Eng [Internet]. 2020 Jan 21;11. Available from:  
444 <https://journals.sagepub.com/doi/10.1177/2041731420921482>
- 445 13. Hoshiba T, Yunoki S. Comparison of decellularization protocols for cultured cell-derived extracellular



- 446 matrix—Effects on decellularization efficacy, extracellular matrix retention, and cell functions. *J Biomed*  
447 *Mater Res Part B Appl Biomater* [Internet]. 2023 Jan 19;111(1):85–94. Available from:  
448 <https://onlinelibrary.wiley.com/doi/10.1002/jbm.b.35135>
- 449 14. El Soury M, García-García ÓD, Moretti M, Perroteau I, Raimondo S, Lovati AB, et al. Comparison of  
450 Decellularization Protocols to Generate Peripheral Nerve Grafts: A Study on Rat Sciatic Nerves. *Int J Mol*  
451 *Sci* [Internet]. 2021 Feb 27;22(5):2389. Available from: <https://www.mdpi.com/1422-0067/22/5/2389>
- 452 15. Simsa R, Padma AM, Heher P, Hellström M, Teuschl A, Jenndahl L, et al. Systematic in vitro comparison of  
453 decellularization protocols for blood vessels. Soncini M, editor. *PLoS One* [Internet]. 2018 Dec  
454 17;13(12):e0209269. Available from: <https://dx.doi.org/10.1371/journal.pone.0209269>
- 455 16. Nahumi A, Peymani M, Asadi A, Abdolmaleki A, Panahi Y. Decellularized tracheal scaffold as a promising  
456 3D scaffold for tissue engineering applications. *Tissue Cell* [Internet]. 2023 Dec;85:102258. Available from:  
457 <https://linkinghub.elsevier.com/retrieve/pii/S004081662300246X>
- 458 17. Jahanvar M, Zahri S, Abdolmaleki A, Asadi A. Evaluation of Decellularized Sheep Kidney Scaffolds for  
459 Renal Tissue Engineering: Biocompatibility and Stem Cell Differentiation Potential. *Tissue Cell* [Internet].  
460 2024 Nov;102594. Available from: <https://linkinghub.elsevier.com/retrieve/pii/S0040816624002957>
- 461 18. Vilaça-Faria H, Noro J, Reis RL, Pirraco RP. Extracellular matrix-derived materials for tissue engineering  
462 and regenerative medicine: A journey from isolation to characterization and application. *Bioact Mater*  
463 [Internet]. 2024 Apr;34:494–519. Available from:  
464 <https://linkinghub.elsevier.com/retrieve/pii/S2452199X24000045>
- 465 19. Rayat Pishch H, Nojabaei FS, Darvishi A, Rayat Pishch A, Sani M. Cardiac tissue engineering: an emerging  
466 approach to the treatment of heart failure. *Front Bioeng Biotechnol* [Internet]. 2024;12:1441933. Available  
467 from: <http://www.ncbi.nlm.nih.gov/pubmed/39211011>
- 468 20. Liu W, Zhang X, Jiang X, Dai B, Zhang L, Zhu Y. Decellularized extracellular matrix materials for treatment  
469 of ischemic cardiomyopathy. *Bioact Mater* [Internet]. 2024 Mar;33:460–82. Available from:  
470 <https://linkinghub.elsevier.com/retrieve/pii/S2452199X23003304>
- 471 21. Moroni F, Mirabella T. Decellularized matrices for cardiovascular tissue engineering. *Am J Stem Cells*  
472 [Internet]. 2014;3(1):1–20. Available from: <http://www.ncbi.nlm.nih.gov/pubmed/24660110>
- 473 22. del Monte-Nieto G, Fischer JW, Gorski DJ, Harvey RP, Kovacic JC. Basic Biology of Extracellular Matrix  
474 in the Cardiovascular System, Part 1/4. *J Am Coll Cardiol* [Internet]. 2020 May;75(17):2169–88. Available  
475 from: <https://linkinghub.elsevier.com/retrieve/pii/S0735109720345903>
- 476 23. Sharma D, Ferguson M, Kamp TJ, Zhao F. Constructing biomimetic cardiac tissues: a review of scaffold  
477 materials for engineering cardiac patches. *Emergent Mater* [Internet]. 2019 Jun 3;2(2):181–91. Available  
478 from: <http://link.springer.com/10.1007/s42247-019-00046-4>

- 479 24. Das P, Singh YP, Mandal BB, Nandi SK. Tissue-derived decellularized extracellular matrices toward  
480 cartilage repair and regeneration. In 2020. p. 185–221. Available from:  
481 <https://linkinghub.elsevier.com/retrieve/pii/S0091679X19301359>
- 482 25. Guo X, Liu B, Zhang Y, Cheong S, Xu T, Lu F, et al. Decellularized extracellular matrix for organoid and  
483 engineered organ culture. *J Tissue Eng [Internet]*. 2024 Jan 28;15. Available from:  
484 <https://journals.sagepub.com/doi/10.1177/20417314241300386>
- 485 26. Kawecki M, Łabuś W, Klama-Baryla A, Kitala D, Kraut M, Glik J, et al. A review of decellularization  
486 methods caused by an urgent need for quality control of cell-free extracellular matrix' scaffolds and their  
487 role in regenerative medicine. *J Biomed Mater Res Part B Appl Biomater [Internet]*. 2018 Feb  
488 14;106(2):909–23. Available from: <https://onlinelibrary.wiley.com/doi/10.1002/jbm.b.33865>
- 489 27. Nawaz M, Shah N, Zanetti BR, Maugeri M, Silvestre RN, Fatima F, et al. Extracellular Vesicles and Matrix  
490 Remodeling Enzymes: The Emerging Roles in Extracellular Matrix Remodeling, Progression of Diseases  
491 and Tissue Repair. *Cells [Internet]*. 2018 Oct 13;7(10):167. Available from: [https://www.mdpi.com/2073-](https://www.mdpi.com/2073-4409/7/10/167)  
492 [4409/7/10/167](https://www.mdpi.com/2073-4409/7/10/167)
- 493 28. Leonard AK, Loughran EA, Klymenko Y, Liu Y, Kim O, Asem M, et al. Methods for the visualization and  
494 analysis of extracellular matrix protein structure and degradation. In 2018. p. 79–95. Available from:  
495 <https://linkinghub.elsevier.com/retrieve/pii/S0091679X17301267>
- 496 29. DiVincenti L, Westcott R, Lee C. Sheep (*Ovis aries*) as a model for cardiovascular surgery and management  
497 before, during, and after cardiopulmonary bypass. *J Am Assoc Lab Anim Sci [Internet]*. 2014  
498 Sep;53(5):439–48. Available from: <http://www.ncbi.nlm.nih.gov/pubmed/25255065>
- 499 30. Banstola A, Reynolds JNJ. The Sheep as a Large Animal Model for the Investigation and Treatment of  
500 Human Disorders. *Biology (Basel) [Internet]*. 2022 Aug 23;11(9). Available from:  
501 <http://www.ncbi.nlm.nih.gov/pubmed/36138730>
- 502 31. Lu TY, Lin B, Kim J, Sulliyam M, Tobita K, Salama G, et al. Repopulation of decellularized mouse heart  
503 with human induced pluripotent stem cell-derived cardiovascular progenitor cells. *Nat Commun [Internet]*.  
504 2013 Aug 13;4(1):2307. Available from: <https://www.nature.com/articles/ncomms3307>
- 505 32. Ott HC, Matthiesen TS, Goh SK, Black LD, Kren SM, Netoff TI, et al. Perfusion-decellularized matrix:  
506 using nature's platform to engineer a bioartificial heart. *Nat Med [Internet]*. 2008 Feb 13;14(2):213–21.  
507 Available from: <https://www.nature.com/articles/nm1684>
- 508 33. Weymann A, Patil NP, Sabashnikov A, Jungebluth P, Korkmaz S, Li S, et al. Bioartificial Heart: A Human-  
509 Sized Porcine Model – The Way Ahead. Benedetto U, editor. *PLoS One [Internet]*. 2014 Nov  
510 3;9(11):e111591. Available from: <https://dx.plos.org/10.1371/journal.pone.0111591>

512

513

514

515

516

517

518

519

520

Preprint